Metastable anisotropy orientation of nematic quantum Hall fluids

Daniel G. Barci[1] and Zochil González Arenas[2]
[1]*Departamento de Física Teórica, Universidade do Estado do Rio de Janeiro, Rua São Francisco Xavier 524, Rio de Janeiro, Rio de Janeiro 20550-013, Brazil*
[2]*Instituto de Cibernética, Matemática y Física (ICIMAF), Calle 15 # 551 e/ C y D, Vedado, Ciudad de La Habana 10400, Cuba*
(Received 11 March 2008; revised manuscript received 4 June 2008; published 8 August 2008)

We analyze the experimental observation of metastable anisotropy resistance orientation at half-filled quantum Hall fluids by means of a model of a quantum nematic liquid in an explicit symmetry-breaking potential. We interpret the observed "rotation" of the anisotropy axis as a process of nucleation of nematic domains and compute the nucleation rate within this model. By comparing with experiment, we are able to predict the critical radius of nematic bubbles—$R_c \sim 2.6$ μm. Each domain contains about 10^4 electrons.

DOI: 10.1103/PhysRevB.78.085303 PACS number(s): 73.43.−f, 71.10.Hf, 71.10.Pm, 64.60.My

I. INTRODUCTION

Quantum liquid crystals are gapless condensates that spontaneously break rotational and/or translational symmetry. There is by now a large amount of theoretical and experimental works studying these new phases of strongly correlated systems in different realizations such as quantum hall systems,[1] high-T_c superconductors,[2] and heavy fermion compounds.[3]

The two-dimensional quantum smectic[4] (also referred to as stripe phase) is a metallic state that breaks translation invariance in one direction. It was conjectured that this modulated electronic configuration is a good ground state of two-dimensional electron gases (2DEGs) under specific values of an external magnetic field.[1,5–9] In fact, at partial filling factor the system tends to separate into homogeneous fluids with different densities. Coulomb repulsion frustrates this tendency and the system is forced to rearrange itself by lowering its dimensionality.[10,11] Collective excitations of this ground state were computed and anisotropic gapless fermionic correlations—very different from those in the usual theory of Fermi liquids[10–14]—were obtained.

Strong thermal, as well as quantum fluctuations of the stripes, could produce topological defects, dislocations, or disclinations that, under appropriate circumstances, can melt the stripe order into an homogeneous but anisotropic liquid.[15] This state is called the quantum nematic state[16,17] and it is probably the best candidate[18,19] to explain the anisotropies observed in 2DEG at half-filled Landau levels.[8,9] In fact, experiments are compatible with the interpretation of a spontaneous rotational symmetry breaking at approximately 150 mK and a weak native potential, responsible for aligning the principal-axis resistance, of the order of 1 mK per electron.[20] On the other hand, no pinning was detected in the $I-V$ curves, which suggests a liquid state rather than periodical arrays.

Some models[21] were proposed to understand the native symmetry-breaking potential responsible for the alignment of the anisotropy. However, the origin of this potential remains unknown. In a recent experiment,[22] the structure of the native potential was studied on highly mobility samples over a large scale of temperatures and magnetic fields. A nontrivial behavior of the resistance anisotropy as a function of temperature and filling factor was reported. It was found that the "easy" direction (the direction with lower resistivity) can be aligned along the $\langle 1\bar{1}0\rangle$ or the $\langle 110\rangle$ crystallographic axes of the host GaAs structure. The actual direction preferred by the system depends on the filling factor and on the in-plane magnetic field. These directions can be interchanged according to the magnetic-field sweep in such a way that an interesting hysteresis pattern (typical of metastability) comes up close to half filling. Moreover, to confirm the picture of a bistable potential, Cooper *et al.*[22] were able to quench the system in a metastable state (say the easy direction along $\langle 110\rangle$). Then, they observed the slow relaxation to the equilibrium state, aligned with the axis $\langle 1\bar{1}0\rangle$, for several final temperatures.

In this paper, we analyze this result in the framework of a nematic quantum fluid submitted to a two component external potential: one with nematic symmetry and the other with tetragonal symmetry, which is possibly induced by the host GaAs structure.[23] For this purpose, we introduce an XY model, describing an effective quantum nematic phase, with a general external symmetry-breaking potential that produces a two orthogonal minima structure. Within this picture, we assume that the decay of the metastable state can be produced by thermal activation over a potential barrier. We expect that bubbles nucleation of the true ground state into the metastable state, produced by long-wavelength thermal fluctuations, is the main mechanism responsible for the decay. This assumption is reasonable provided that the energy of the critical bubble is much greater than the equilibrium temperature. We will show that this is, in fact, the case for the data in Ref. 22.

We use the Langer[24] homogeneous nucleation theory to compute decay rates of the metastable state. We calculate the critical bubble profile of the model and estimate the critical energy and radius by using two methods: an analytical variational approach and an exact numerical computation. By comparing them with the experiment, we are able to predict the radius of critical domains of the order of 2.6 μm, containing approximately 10^4 electrons. We find that the time evolution of the anisotropy resistance observed in Ref. 22 is in agreement with the picture of nucleation of nematic domains (with the directors pointing along a stable direction) in a metastable nematic background with the principal axis aligned in the perpendicular direction. We also show that the

homogeneous nucleation theory is good enough to make estimations at first order, while the thin wall approximation is not quite accurate. Our calculations predict that the domains have broad walls in the actual experimental conditions.

We present our model of quantum nematic in an external potential in Sec. II. To make this paper self-contained and to fix notations, we briefly review the theory of two-dimensional homogeneous nucleation in our context in Sec. III. Then, in Sec. IV, we compute the decay rate, the critical energy, and the radius of the critical bubble as a function of the parameters of our model by using a variational approach and the thin wall approximation. To check our approximations, we numerically integrate the differential equation, which defines the critical bubble and compare the results with our previous analytical estimations in Sec. V. Finally, we compare our analysis with experimental results in Sec. VI and summarize our conclusions in Sec. VII.

II. *XY* MODEL OF A QUANTUM NEMATIC LIQUID IN A SYMMETRY-BREAKING POTENTIAL

A nematic state is a homogeneous orientational ordered state with the forward and backward directions identified. That means that if the system has a preference axis orientated along an angle θ, then the state has the nematic symmetry $\theta \rightarrow \theta+\pi$. In two dimensions, this property is encoded in the definition of the complex order parameter $Q=\rho\ e^{i2\theta}$, where the argument 2θ guarantees the nematic symmetry. Close to the isotropic-nematic transition, we can expand the free energy in powers of Q,

$$F(Q)=\frac{1}{2}\int d^2x\vec{\nabla}Q\cdot\vec{\nabla}Q^* + \frac{1}{V}\int d^2x\left[\frac{1}{2}a_2QQ^*+\frac{1}{4}a_4(QQ^*)^2\right]+V(hQ)+\ldots, \tag{2.1}$$

where a_2 and a_4 are arbitrary constants, which depend on the microscopic details of the system. $V(hQ)$ is an explicit symmetry-breaking term, which depends on some external field h. Different from three dimensions, in the two-dimensional Ginzburg-Landau expansion of the nematic order parameter, there is no cubic term.

In the absence of external symmetry-breaking potential, the modulus of the order parameter spontaneously gets a nonzero value ρ for $a_2<0$, while the angle θ remains arbitrary. In two dimensions, the angle fluctuations are logarithmically divergent.[25] Therefore, in the absence of external fields there is no true order but there is algebraic quasi-long-range order. However, in the presence of a small symmetry-breaking potential, this divergence is removed. In this case, even small values of the external potential can produce big values of the order parameter due to the huge susceptibility of this transition.

The dynamics of the lowest energy modes is governed by the coarse-grained Hamiltonian [as usual, we have assumed at low temperatures a constant modulus of the order parameter in Eq. (2.1)],

$$H=\int d^2x\frac{J}{2}|\vec{\nabla}\theta|^2+V(\theta), \tag{2.2}$$

where J is the typical energy scale of the Kosterlitz-Thouless[25] phase transition and $V(\theta)$ is an arbitrary potential that explicitly breaks rotation invariance but preserves the nematic symmetry in such a way that $V(\theta)=V(\theta+\pi)$.

It is possible to parametrize this potential in terms of its even Fourier coefficients

$$V(\theta)=\sum_n h_{2n}\cos(2n\theta), \tag{2.3}$$

where h_2 is related with a nematic external field, h_4 is a symmetry-breaking coefficient with tetragonal symmetry, and so on.

This model, with $n=1$ in Eq. (2.3), was used to fit the isotropic/anisotropic transition of a Hall liquid at $\nu=9/2$ filling factor by means of Monte Carlo simulations.[18] It was shown that the general picture of a nematic liquid in a small symmetry-breaking field correctly describes the transition. To use this model for fitting experimental data, it is necessary to relate the nematic order parameter with observables. In Ref. 18, it was shown that the relation

$$\frac{\rho_{xx}-\rho_{yy}}{\rho_{xx}+\rho_{yy}}=\langle\cos 2\theta\rangle+\ldots \tag{2.4}$$

is a good approximation over a huge temperature range, except at extremely low temperatures where quantum fluctuations become important. In Eq. (2.4), ρ_{xx} and ρ_{yy} are the measured longitudinal resistivities in the x and y directions, respectively.

In this paper, we adopt the same criteria and study higher harmonics of the external field. For this purpose, we will analyze the effect of the second term $n=2$ in Eq. (2.3). Thus, we will consider a potential of the form

$$V(\theta)=h_2\cos(2\theta)-h_4\cos(4\theta), \tag{2.5}$$

where $h_2>0$ and $h_4>0$ are coefficients that measure the relative weights of the nematic and tetragonal components of the host symmetry-breaking potential. It is interesting to note that, while the term h_2 is somehow mysterious, the term h_4 is not prohibited by symmetry and could be induced by the square structure of the host GaAs.[23]

The net effect of the term h_4 is to introduce local metastable minima for the angular variable θ. We depict the potential for typical values of $h_2<4h_4$ in Fig. 1. The sign of h_4 controls which one of the different minima is metastable and which one is the true ground state. We arbitrarily choose this sign in such a way of having a metastable state at $\theta=n\pi$ and the ground state at $\theta=\pi(2n+1)/2$ with $n=0,\pm1\ldots$. On the other hand, the potential has maxima at $\cos(2\theta_{\mathrm{Max}})=h_2/(4h_4)$.

The energy difference between the stable and metastable minima is $2h_2$, while h_4 is related with the height of the energy barrier, in fact,

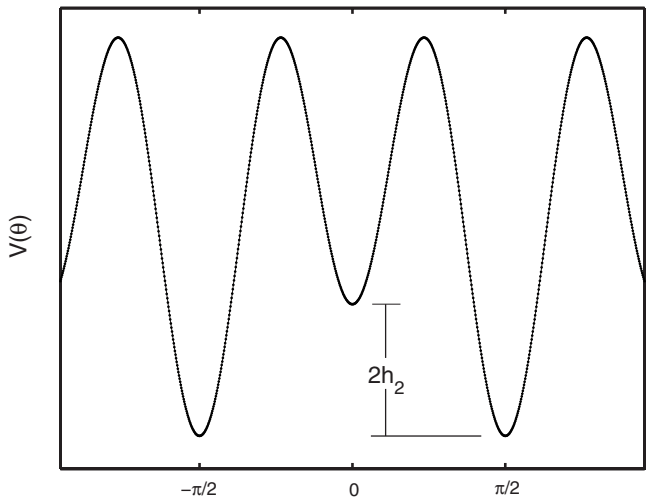

FIG. 1. Potential of Eq. (2.3) with $h_2<4h_4$. The metastable states are at $\theta=n\pi$, while the true ground state is aligned with $\theta=\pi(2n+1)/2$ with $n=0,\pm1\ldots$. Maxima are taken at $\cos(2\theta_{\mathrm{Max}})=h_2/(4h_4)$. The energy difference between minima is $2h_2$ and the height of the barrier in relation to h_4 through Eq. (2.6).

$$V(\theta_{\mathrm{Max}})-V(0)=\frac{h_2^2+2h_4^2+h_2h_4}{h_4}, \tag{2.6}$$

which in the limit of quasidegenerate minima reduces to $V(\theta_{\mathrm{max}})-V(0)=2h_4$.

With this potential it would be possible, by a quenching process, to prepare the system in a metastable phase—for instance, a nematic state with principal axis pointing in the $\theta=0$ direction. In these conditions, we would expect that long-wavelength thermal fluctuations could produce nucleation of nematic domains with principal axis in the perpendicular direction $\theta=\pi/2$. Therefore, we should see that the anisotropy of the resistivity "rotates" or changes in time from one direction to its perpendicular one as it has been observed.[22]

III. TWO-DIMENSIONAL BUBBLE NUCLEATION

One of the possible mechanisms for thermal activated decaying is the nucleation[26] of ground-state domains in a homogeneous metastable state, which fills all the available area. The dynamics is determined by the domain's energy that, in general, is a competition between a bulk contribution (proportional to its area) and a boundary term (proportional to its perimeter).

Consider, for instance, a bubble with spherical symmetry of radius R as depicted in Fig. 2. In the thin wall approximation, that is, when the width of the wall is much smaller than the radius, the boundary and bulk contributions to the energy are well defined,

$$E(R)=-\pi\Delta\mathcal{F}R^2+2\pi\sigma R+\ldots, \tag{3.1}$$

where $\Delta\mathcal{F}$ is the energy difference between the stable and metastable states per unit area, σ is the surface tension, and the ellipsis indicates subleading order in the thin wall approximation.

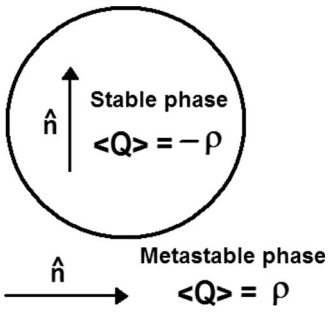

FIG. 2. Sketch of a symmetrical bubble which contains a nematic liquid with the director pointing in the $\theta=\pi/2$ direction. It is embedded in a metastable state composed of a nematic liquid with the director pointing to $\theta=0$. ρ is the modulus of the nematic order parameter and $\hat{n}$ is the director.

While for small radius the positive boundary term dominates the energy; for large R, the negative bulk contribution dominates. Due to this competition, there is a critical radius $R_c=\sigma/\Delta\mathcal{F}$, where the energy has a maximum $E_c=\pi\sigma^2/\Delta\mathcal{F}$ and the critical bubble is at unstable equilibrium. The supercritical bubbles ($R>R_c$) will grow until filling all the area with the ground state. On the other hand, the subcritical bubbles ($R<R_c$) will shrink and finally disappear. Both contributions are important in a phase transition since the actual mechanism is given by random long-wavelength thermal fluctuations, which generate all types of bubbles. Some of them will grow and others will shrink. In this picture, the transition is completed when the true ground state percolates the metastable one. The relative importance of these contributions depends on the probability of fluctuations and on the growth rate of the supercritical bubbles,

$$\Omega=\frac{d}{dt}\left[\ln\left|\frac{R(t)}{R_c}-1\right|\right]. \tag{3.2}$$

The important quantity to study nucleation is the nucleation rate per unit of area. In the homogeneous nucleation theory of Langer,[24] this quantity is given by $\Gamma=\Omega\mathcal{D}\exp(-E_c/T)$, where E_c is the energy of a critical bubble, T is the final equilibrium temperature, Ω is the growth rate of a slightly supercritical bubble,[27] and the prefactor $\mathcal{D}$ comes from the computation of fluctuations around the critical bubble profile.

The computation of Ω and $\mathcal{D}$ from microscopic quantum models is a very difficult task (see Ref. 27 and references therein). However, it was shown[28] that in two dimensions and in the thin wall approximation ($\Delta\mathcal{F}\to0$), these quantities can be cast in terms of the macroscopic parameter $\Delta\mathcal{F}$,

$$\Gamma=\frac{\Delta\mathcal{F}}{2\pi\hbar}e^{-E_c/T}. \tag{3.3}$$

Interestingly, due to its two-dimensional character, this expression has no corrections in powers of the thin wall adimensional parameter[28] $\Delta\mathcal{F}T/\sigma^2$.

Homogeneous nucleation theory is reliable provided $E_c\gg T$. For $E_c\sim T$, small amplitude thermal fluctuations could trigger the phase transition and nucleation and spin-

odal decomposition can no longer be distinguished.

Provided that the conditions for homogeneous nucleation are satisfied, the probability of nucleating several bubbles at the same time is very small. We can estimate the typical time to complete a transition as the time of a simple nucleation event. Then,

$$\tau = \frac{1}{\Gamma A} = \frac{2\pi\hbar}{\Delta\mathcal{F}A} e^{E_c/T}, \tag{3.4}$$

where τ is the time estimated to complete the transition, Γ is the nucleation rate per unit of area, and A is the total area of the sample considered.

This "static" approach will be sufficient for the purpose of this paper. However, time dependent corrections to Langer theory can be evaluated using out of equilibrium Shwinger-Keldish techniques.[27]

In the next section, we will compute the time τ as well as the coefficients $\Delta\mathcal{F}$ and σ in terms of the parameters of our model J, h_2, and h_4.

IV. NEMATIC CRITICAL BUBBLES AND THE THIN WALL APPROXIMATION

A critical bubble is a radially symmetric static field configuration that solves the following differential equation:

$$\nabla^2\theta - \frac{1}{J}\frac{\partial V(\theta)}{\partial\theta} = 0, \tag{4.1}$$

with the boundary conditions $\lim_{r\to\infty}\theta(r)=0$ and $\lim_{r\to\infty}\theta'(r)=0$. $V(\theta)$ is the potential of Eq. (2.5) (Fig. 1).

Such a solution describes a "bubblelike" configuration, which starts close to the true ground state $\theta=\pi/2$ and reaches the metastable state $\theta=0$ at asymptotically large distances. The change from the stable to the metastable state occurs around the critical radius R_c and over a distance ξ, which defines the wall thickness of the bubble. We depict a typical profile of a critical bubble and we also draw the square derivative of the profile in Fig. 3. The maximum of the derivative defines the critical radius and the width of the peak is a measure of the bubble wall thickness that, as we will show, is related to the nematic correlation length in the metastable phase.

Equation (4.1) is an extremely difficult differential equation to solve analytically and we will show a numerical treatment in Sec. V. However, it is possible to have some insight of its behavior through a variational analysis. The idea is to propose a reasonable ansatz for the solution by considering the critical radius and the wall thickness as variational parameters. Then, we determine these parameters by extremizing the critical energy. We make the following ansatz:

$$\theta_b(r) = \frac{\pi}{4}\left[1 - \tanh\left(\frac{r-R_c}{\xi}\right)\right], \tag{4.2}$$

where the radius R_c and the wall thickness ξ will be determined by extremizing the energy.

The form of this function is inspired in the problem of an asymmetric quartic potential.[29–31] In that case, Eq. (4.2) is the exact solution of Eq. (4.1) for the one-dimensional problem and, for higher dimensions, it is the correct form in the thin wall approximation $\xi/R_c \ll 1$.[27] Although our potential is much more complicated than a simple quartic one, we expect to grasp the general behavior and the correct order of magnitude with this ansatz. Of course, a variational technique is not a well-controlled approximation; thus, in Sec. V, we compare our variational analytical results with a numerical treatment of Eq. (4.1). Just to have some feeling on the approximation, we compare the variational profile of Eq. (4.2) with the exact one obtained from direct numerical integration of Eq. (4.1) in Fig. 4.

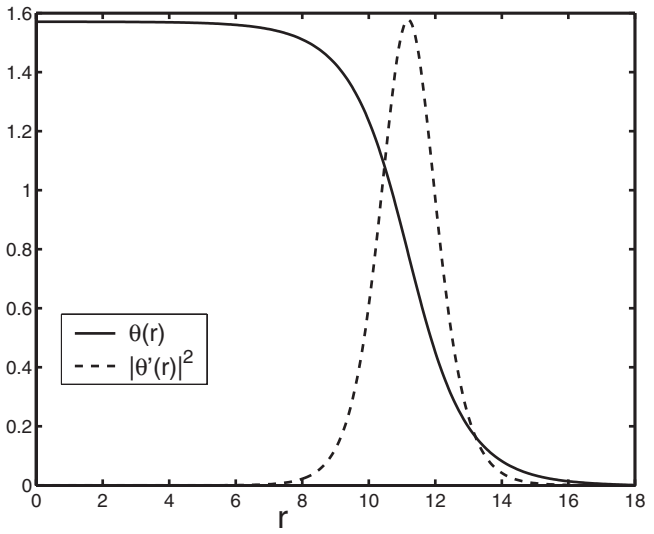

FIG. 3. Typical radial symmetric bubble profile that solves Eq. (4.1). The continuous line represents the bubble configuration, which starts close to the true ground state $\theta=\pi/2$ and reaches the metastable state $\theta=0$ at asymptotically large radial distance. The dash line is the square derivative (properly rescaled) that defines the critical radius and the wall thickness.

Substituting Eq. (4.2) into the Hamiltonian Eq. (2.2), we have the energy of the bubble as a function of the variational parameters,

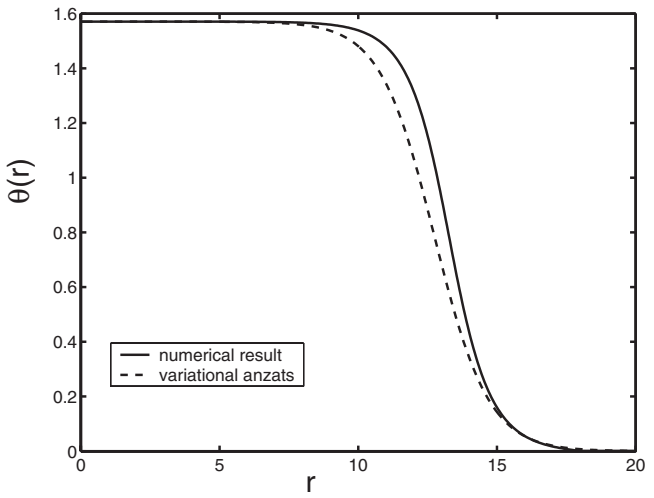

FIG. 4. Comparison between a numerical solution of Eq. (4.1) (continuous line) and the variational ansatz Eq. (4.2) (dash line).

$$E(R_c,\xi) = \int d^2x \frac{J}{2}|\vec{\nabla}\theta_b(r,R_c,\xi)|^2 + V(\theta_b(r,R_c,\xi)). \tag{4.3}$$

Integrating to leading order in ξ/R_c we find an expression similar to Eq. (3.1),

$$E(R_c,\xi) = -\pi\Delta\mathcal{F}R_c^2 + 2\pi\sigma(\xi)R_c + O[(\xi/R_c)^2], \tag{4.4}$$

where

$$\Delta\mathcal{F} = V(0) - V(\pi/2) = 2h_2, \tag{4.5}$$

essentially comes from the integral of the potential. On the other hand, $\sigma(\xi)$ has contributions from both terms of the integral and is given by

$$\sigma(\xi) = \frac{\pi^2}{32}\left[\frac{\pi}{2}\frac{J}{\xi} + 0.39V''(0)\xi\right]. \tag{4.6}$$

The first term comes from the gradient contribution and grows when the thickness narrows. On the contrary, the second term, which comes from the potential, is a linear increasing function of ξ. Therefore, we fix this parameter by looking for a stationary solution,

$$\frac{\partial E(R_c,\xi)}{\partial\xi} = 2\pi R_c\frac{d\sigma}{d\xi} = 0, \tag{4.7}$$

and obtain the optimal value,

$$\xi = 2\sqrt{\frac{J}{V''(0)}} = \frac{J^{1/2}}{\sqrt{4h_4 - h_2}}, \tag{4.8}$$

which is two times the correlation length on the metastable phase. With this value for the thickness, the superficial tension gets the simplest form,

$$\sigma \sim \frac{J}{\xi} = J^{1/2}\sqrt{4h_4 - h_2}. \tag{4.9}$$

Now, we can determine the critical radius R_c by imposing

$$\frac{\partial E(R_c,\xi)}{\partial R_c} = -2\pi R_c\Delta\mathcal{F} + 2\pi\sigma(\xi) = 0. \tag{4.10}$$

We have, in this way,

$$R_c = \frac{\sigma}{\Delta\mathcal{F}} = \frac{J^{1/2}}{2}\frac{\sqrt{4h_4 - h_2}}{h_2}. \tag{4.11}$$

Finally, plugging $\Delta\mathcal{F}$, σ, and R_c into Eq. (4.4), we obtain the energy of the critical bubble,

$$\frac{E_c}{J} = \frac{\pi}{2}\left(\frac{4h_4}{h_2} - 1\right). \tag{4.12}$$

It is necessary to have in mind that the thin wall approximation also imposes restrictions on the values of h_2 and h_4, since

$$\frac{\xi}{R_c} = \pi\frac{J}{E_c} = 2\left(\frac{4h_4}{h_2} - 1\right)^{-1} \ll 1. \tag{4.13}$$

This completes our estimation of relevant dynamical quantities in terms of the parameters of our model in the thin wall approximation.

V. NUMERICAL CALCULATIONS

In order to check the range of validity of our variational approach, we numerically evaluate the bubble profile and the energy.

Assuming a solution with radial symmetry and rescaling the variables with the magnetic length ℓ_c as

$$h_{2,4} \to h_{2,4}\frac{J}{\pi\ell_c^2}, \quad r^2 \to r^2\pi\ell_c^2, \tag{5.1}$$

we find the adimensional equation,

$$\frac{d^2\theta}{dr^2} + \frac{1}{r}\frac{d\theta}{dr} + 2h_2\sin(2\theta) - 4h_4\sin(4\theta) = 0, \tag{5.2}$$

with the boundary conditions $\lim_{r\to\infty}\theta(r)=0$ and $\lim_{r\to\infty}\theta'(r)=0$.

To solve this equation, we transform the boundary-value problem into an initial condition problem and use the shooting method to seek for solutions. In this method, one shoots the initial derivative, integrates the equation with a Runge-Kutta method of order 4, and (according to the accuracy to match the boundary values) the initial conditions are corrected. This procedure is iterated looking for convergence.

To actually solve the equation, we need to fix h_2 and h_4. There is by now extended experimental work in different samples and regions of magnetic field and density that clearly shows that, while the anisotropy appears around $T=150$ mK, the energy scale of the aligning potential is about 1 mK per electron. In our model, this is compatible with values of h_2 and h_4 of the order of 10^{-2} in units of $J/\pi\ell_c^2$. For instance, in Ref. 18, the isotropic/anisotropic transition at $\nu=9/2$ was successfully fitted with a value of $h_2=0.05$. Of course, the specific value may change for different samples and for different filling factors and in-plane magnetic fields. As we have stated before, due to the bidimensionality, the prefactor in the decay rate [Eq. (3.3)] depends just on the energy difference between the minima (say $2h_2$) and not on the height of the barrier, which is proportional to h_4. This means that for a given value of the decay time, the energy of the critical bubble only has a logarithmic dependence on h_2. Then, what actually matters for the calculation of the energy of the critical bubble is the order of h_2 and not its precise value. For this reason, we will fix a reasonable value of h_2 and we will make the numerical calculations for several values of h_4 in the range of 10^{-2}. When comparing with experiments, we will comment again on these values and will show the robustness of the results for small changes of these quantities.

In Fig. 5 we show a set of solutions with fixed $h_2=0.02$ for several values of h_4, while in Fig. 6 the square modulus of the derivatives are depicted for the same values of the parameters. First, we observe the general features of a critical bubble described in Secs. I and IV as expected. All solutions begin near $\theta=\pi/2$ and asymptotically go to $\theta=0$. The

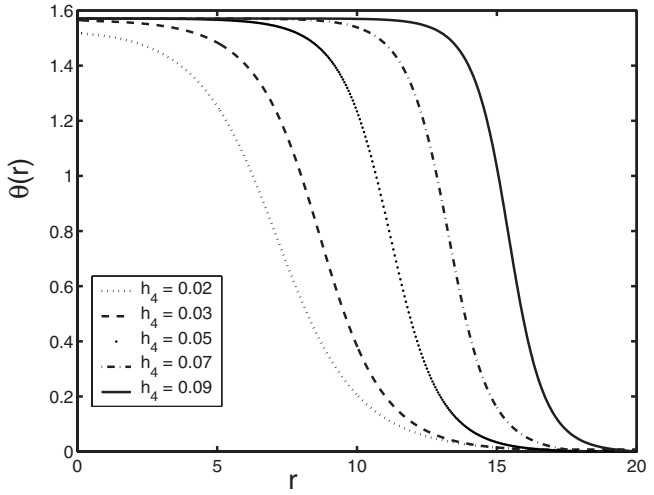

FIG. 5. Bubble profiles for different values of h_4. We have fixed h_2=0.02 for all solutions. r is measured in units of $\sqrt{\pi}\ell_c$ and h_4 in units of $J/\pi\ell_c^2$.

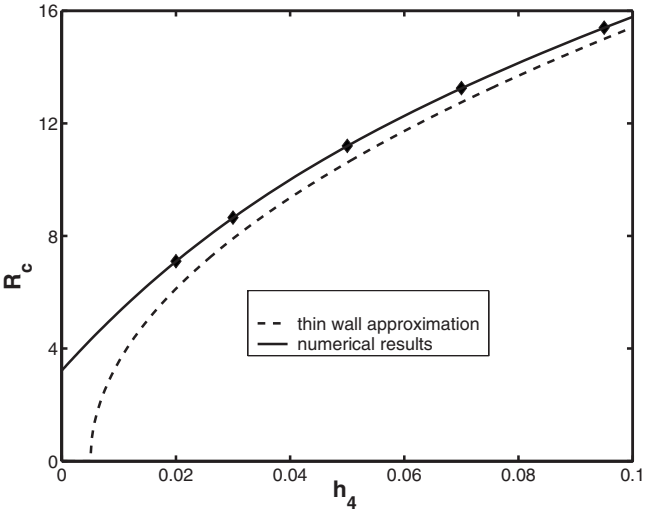

FIG. 7. Critical radius as a function of h_4. The continuous line is a polynomial fit. The dash line is the critical radius in the thin wall approximation calculated with Eq. (4.11). We have fixed h_2=0.02. R_c is measured in units of $\sqrt{\pi}\ell_c$ and h_4 in units of $J/\pi\ell_c^2$.

critical radius R_c can be read from the position of the maxima of Fig. 6 and we can estimate the wall thickness as the width of peaks at some arbitrary fixed height (half the peak height, for instance). According to Sec. IV, we see that R_c is an increasing function of h_4 and the greater h_4 the smaller the wall thickness. We collect this information in Fig. 7, where we draw the critical radius as a function of h_4. The continuous line connecting the points is a polynomial fit. We also draw with a dash line the function $R_c(h_4)$ given by Eq. (4.11). Interestingly (except for very low values of h_4), the variational result reasonably agrees with the exact result; the greater h_4 the better the approximation.

Finally, we compute the energy of each critical bubble by numerically integrating Eq. (4.3). In Fig. 8, we show the energy as a function of the critical radius. The continuous line is a polynomial fit of second order. Note that we are perfectly fitting five points with a second-order polynomial. The reason for that is simple: The critical energy can be cast in terms of the critical radius as $E_c=\Delta\mathcal{F}\pi R_c^2$. We have estimated this parameter to be $\Delta\mathcal{F}=2h_2$. Therefore, we expect a quadratic dependence of the form $E_c=a_2R_c^2$, with the quadratic coefficient given by $a_2=2h_2\pi$. We have found a fitting value a_2=0.1257, which is in excellent agreement with the thin wall estimation with the value h_2=0.02 fixed for all the critical bubbles. It seems striking to compare Figs. 7 and 8. While in Fig. 8 the exact results match thin wall calculations almost perfectly, in Fig. 7 we see a clear deviation. The reason is that in determining $\Delta\mathcal{F}$, the only contribution comes from the second term of Eq. (4.3). The contribution of order R_c^2 essentially comes from the constant part of the bubble profile and our variational function estimates this area quite well. Indeed, this is the only source of error in the results in Fig. 8 and, for this reason, the numerical calculations and the variational estimations match almost perfectly. On the other

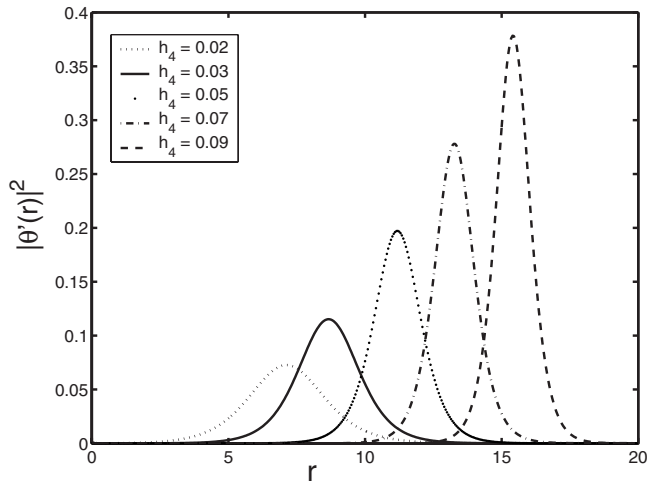

FIG. 6. Wall profiles for different values of h_4. We have fixed h_2=0.02 for all solutions. r is measured in units of $\sqrt{\pi}\ell_c$ and h_4 in units of $J/\pi\ell_c^2$.

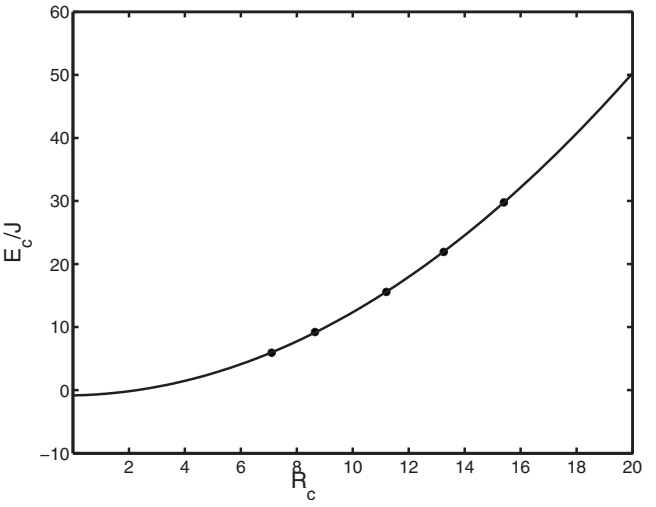

FIG. 8. Critical energy in units of J as a function of the critical radius R_c expressed in units of $\sqrt{\pi}\ell_c$. The continuous line is a polynomial fit of order two.

hand, for the estimation of σ (necessary to evaluate the critical radius) [see Eq. (4.11)], we have two contributions [see Eq. (4.6)]. Both of them come from the bubble wall and, as we can see from Fig. 4, our variational ansatz is not so good in that region. However, as it is shown in Fig. 7, the approximation gets better as the value of h_4 grows, since the barrier height increases and, consequently, the wall gets thinner in this limit.

VI. EXPERIMENT INTERPRETATION

In this section we analyze the experimental results of Ref. 22 in the context of our model of nematic nucleation. The main purpose of this section is to analyze whether the above mentioned data can be interpreted as thermal activation over a barrier and if the homogeneous nucleation theory of Langer is applicable. Moreover, we want to check the idea of a nematic liquid proposed earlier[1,18] to describe the ground-state properties of these systems. To reach this aim, we need to make not only qualitative comparisons with experiment but also concrete predictions—especially about the size of the nematic domains and walls—in order to further check this picture.

In Ref. 22, Cooper *et al.* showed clear evidences of metastable behavior in the resistance anisotropy orientation of very clean two-dimensional electron gas (2DEG). The measurements were done in a square sample of area 25 mm^2 and density $N_s=3\times10^{11}$ cm^{-2}. The main result was that the "hard" and easy directions of the longitudinal resistance depend (at half filling, $\nu=9/2,11/2,13/2\ldots$) on the magnetic-field sweep. A typical hysteresis diagram associated with metastability was shown and, in the same work, the authors were able to "quench" the state into a metastable direction and to follow the slow relaxation to the equilibrium. The decay rate strongly depended on temperature and on filling factor.

The procedure for analyzing the experiment in the context of our model is the following: We take three measured quantities from the experiment; the time needed to complete the anisotropy "rotation," the equilibrium temperature at which the decay was observed, and the critical temperature for the isotropic/anisotropic transition. With this input, we compute the energy of the critical bubble by inverting Eq. (3.4). Note that this calculation is model independent and its result gives us information about the applicability of Langer theory. With this value of the energy, we estimate the critical radius R_c from Fig. 8. The value of h_2, as was explained before, was taken from several previous experiments and theoretical fittings and the value of the parameter h_4 is predicted from Fig. 7.

In Table I we have collected the experimental results for $\nu=13/2$ in the first two columns. τ is an estimation of the typical time to complete the transition and T is the equilibrium temperature at which the time evolution was witness.

Assuming that the main mechanism is thermal activation, it is immediate to estimate, from this data, the value of the critical energy by using Eq. (3.4). The area was taken from the experiment and we have fixed the value of $h_2=0.02J/(\pi\ell_c^2)$. Due to the logarithmic dependence, the critical energy is not sensible to this particular value but just to its order. We have fixed it by considering that the strength of the native symmetry-breaking potential is about 1 mK per electron.[20] The results are depicted in the third column of Table I.

TABLE I. Summary of experimental results and theoretical predictions. T is the equilibrium temperature of the final state, τ is the typical time that the transition takes to be completed, E_c is the energy of the critical bubble, R_c is the critical radius, ℓ_c is the magnetic length, and h_4 is the tetragonal component of the native potential measured in units of $J/\pi\ell_c^2$.

T (mK)	τ (s)	E_c/T	E_c/J	$R_c/\sqrt{\pi}\ell_c$	h_4
50	3.6×10^4	51	5.7	6.8	0.020
70	6×10^2	47	7.3	7.6	0.023
90	1	41	8.2	8.1	0.026

The first observation is that E_c/T takes values between 40 and 50. Therefore, the homogeneous nucleation theory of Langer is a reasonable approximation—at least for first-order estimations since $E_c/T\gg1$. Note that this value of the energy corresponds to $E_c\sim3K$.

The next step is to compute E_c/J. The stiffness J can be considered of the same order of the isotropic/anisotropic transition $J=\alpha T_c$, where α is a constant of order one and T_c is the critical temperature for the isotropic/anisotropic transition. While T_c is an experimental data, α should be computed from the model. The order of $T_c\sim150$ mK is not difficult to obtain; a more accurate number is generally more involved since the transitions are rounded by disorder and other effects. On the other hand, the value of α for our model is not simple to compute. When ignoring the small symmetry-breaking potential, the renormalization-group analysis of the Kosterlitz-Thouless transition[15] gives an estimation of $\alpha\sim3$. Moreover, Monte Carlo simulations of the full model[18] (fitting the experimental data of Ref. 8) (at $\nu=9/2$) give a reduced value of $\alpha\sim1.1$. For the estimation of E_c/J, we have used $T_c\sim150$ mK, which is reasonable for $\nu=13/2$ (note in Ref. 22 that at 100 mK the anisotropy is completely developed at this filling factor), and the value of α obtained from a renormalization-group analysis. These values are shown in the fourth column of Table I.

Now we are ready to predict the value of the critical radius and the parameter h_4 by using the numerical calculations of Figs. 8 and 7, respectively. We show these results in the last two columns of Table I.

We find for the critical radius $R_c\sim2.6$ μm, where we have considered the magnetic length $\ell_c=197$ Å (at $\nu=13/2$). By taking into account the electronic density of the sample, this value gives an estimation of 10^4 electrons inside the critical bubble. We see that this prediction is completely reasonable since the dimension of the critical domains is big enough to approximately contain ten broken stripes in each domain provided that we consider the Hartree-Fock value of the stripe period[5] as a reasonable estimation. Moreover, the domains are 10^6 times smaller than the size of the sample.

Although the precise value of h_2 was fixed by hand, the size of the critical domain predicted is not very sensible to

that value. In fact, since the critical energy is only logarithmically dependent on h_2 and $E_c=\pi\Delta\mathcal{F}R_c^2$, we see from Eq. (4.5) that $R_c\sim 1/\sqrt{h_2}$. That means that when varying h_2 over a range of reasonable values, the critical radius only changes up to 15%. We also note that the predicted value of h_4 is almost equal to h_2 and shows a very tiny temperature dependence. Recently, it was pointed out[23] that piezoelectricity in GaAl can induce an aligning potential of the form $\cos(4\theta)$. In that work, it was predicted that the barrier between the two degenerated minima is 10^{-4} times the Coulomb energy, which is roughly 1 mK per electron. This value is in complete agreement with the values of h_4 predicted in this paper.

We have repeated the calculations with different values of h_2 and we have found a linear relation $h_2/h_4\sim O(1)$. This is compatible with Eq. (4.12), which (for a fixed value of E_c) predicts the linear dependence in the thin wall approximation (up to logarithmic corrections). Of course, in order to determine a precise value for the parameter h_2, it is necessary to fit the data for all values of temperatures above the critical temperature.

It is important to note that, although the homogeneous nucleation approximation seems to be a reasonable one, the thin wall approximation is not accurate for the regime of this experiment. This fact can be observed in Fig. 7. By using Eq. (4.13) we estimate $\xi/R_c\sim 2/3$. Then, the domain walls are not sharply defined—getting broader on a smooth interphase of approximately 1 μm.

VII. SUMMARY AND DISCUSSIONS

We have analyzed the experimental observation[22] that the native potential, responsible for the resistance anisotropy alignment in quantum Hall fluids at half filling, has a nontrivial structure, which favors two orthogonal directions.

In this framework, we have studied an *XY* model, which describes a nematic fluid in an external symmetry-breaking potential compatible with the nematic symmetry. We have considered the tetragonal coefficient of the Fourier expansion of the potential and we have shown how it can produce two orthogonal local minima structure.

In this picture, we have assumed that the rotation, observed in the anisotropy axis is mainly driven by thermal activation over a barrier. Then, the decay of a metastable direction into the orthogonal direction, which represents the true ground state, is dominated by nucleation of nematic domains.

To compute decay rates, we have used the homogeneous nucleation theory[24] and, after comparing with experiment, we have concluded that it is a reasonable approximation for first-order estimations since $E_c/T\sim 50$ for the data of Ref. 22.

We have implemented an analytical variational approach inspired in the bubble solutions of a quartic potential and we have computed the critical energy and radius in the thin wall approximation. In order to check the quality and the range of applicability of our approximations, we have numerically integrated the critical bubble differential equation and we have computed its energy for a wide range of parameters.

By comparing with the experiment, we were able to predict the radius of the nematic critical domains of the order of $R_c\sim 2.6$ μm; each domain approximately contains 10^4 electrons. However, we found that the width of the wall is quite broad. There is a smooth transition from the true ground state to the metastable state spread in a region of the order of $\xi\sim 1$ μm. Therefore, although the mechanism of homogeneous nucleation seems to be a reasonable assumption, the thin wall approximation is not accurate for the actual regime showed in the data.

The prediction on the size of the critical domains is robust in the sense that it does not strongly depend on the detailed value of h_2. On the other hand, it is quite sensible to the experimental determination of the critical temperature T_c for the isotropic/anisotropic phase transition and to the computation of the stiffness of the *XY* model in the presence of an external field. A Monte Carlo fitting of the complete data, including high temperatures around T_c for different filling factors, would help to improve the accuracy of the predictions of R_c and h_4.

Finally, we would like to point out that, while the mechanism proposed in this paper is in agreement with experiment, it is not the only possibility for its explanation. Indeed, the origin of metastability could be produced from competition between different crystal liquid phases rather than from a native potential or perhaps from combinations of both effects. In a recent paper,[32] it was shown that the competition between nematic and hexatic order parameter leads to a first-order phase transition with a clear signature of metastability in the orientation of the principal axis. The quantum hexatic phase could be produced from the melting of the crystal bubble phase. All these anisotropic states are in fact competing close to half filling, contributing to the interesting complex structures of longitudinal resistivity reported. We hope to report on this possibility soon.

ACKNOWLEDGMENTS

The Brazilian agencies Conselho Nacional de Desenvolvimento Científico e Tecnológico (CNPq) and the Fundação de Amparo à Pesquisa do Estado do Rio de Janeiro (FAPERJ) are acknowledged for their financial support. This work was partially supported by the binational collaboration UERJ-Brazil/ICIMAF-Cuba founded by Centro Latino-Americano de Física (CLAF).

[1] Eduardo Fradkin and Steven A. Kivelson, Phys. Rev. B **59**, 8065 (1999).
[2] V. J. Emery, E. Fradkin, and S. A. Kivelson, Nature (London) **393**, 550 (1998).
[3] R. A. Borzi, S. A. Grigera, J. Farrell, R. S. Perry, S. J. S. Lister, S. L. Lee, D. A. Tennant, Y. Maeno, and A. P. Mackenzie, Science **315**, 214 (2007).
[4] V. J. Emery, E. Fradkin, S. A. Kivelson, and T. C. Lubensky, Phys. Rev. Lett. **85**, 2160 (2000).
[5] A. A. Koulakov, M. M. Fogler, and B. I. Shklovskii, Phys. Rev. Lett. **76**, 499 (1996); M. M. Fogler, A. A. Koulakov, and B. I. Shklovskii, Phys. Rev. B **54**, 1853 (1996); M. M. Fogler and A. A. Koulakov, *ibid.* **55**, 9326 (1997).
[6] R. Moessner and J. T. Chalker, Phys. Rev. B **54**, 5006 (1996).
[7] A. H. MacDonald and Matthew P. A. Fisher, Phys. Rev. B **61**, 5724 (2000).
[8] M. P. Lilly, K. B. Cooper, J. P. Eisenstein, L. N. Pfeiffer, and K. W. West, Phys. Rev. Lett. **82**, 394 (1999).
[9] R. R. Du, D. C. Tsui, H. L. Stormer, L. N. Pfeiffer, K. W. Baldwin, and K. W. West, Solid State Commun. **109**, 389 (1999).
[10] Daniel G. Barci, Eduardo Fradkin, Steven A. Kivelson, and Vadim Oganesyan, Phys. Rev. B **65**, 245319 (2002).
[11] Michael J. Lawler and Eduardo Fradkin, Phys. Rev. B **70**, 165310 (2004).
[12] Daniel G. Barci and Eduardo Fradkin, Phys. Rev. B **65**, 245320 (2002).
[13] A. Lopatnikova, S. H. Simon, B. I. Halperin, and X. G. Wen, Phys. Rev. B **64**, 155301 (2001).
[14] R. Cote and H. A. Fertig, Phys. Rev. B **62**, 1993 (2000).
[15] C. Wexler and A. T. Dorsey, Phys. Rev. B **64**, 115312 (2001).
[16] Vadim Oganesyan, Steven A. Kivelson, and Eduardo Fradkin, Phys. Rev. B **64**, 195109 (2001).
[17] Michael J. Lawler, Daniel G. Barci, Victoria Fernández, Eduardo Fradkin, and Luis Oxman, Phys. Rev. B **73**, 085101 (2006).
[18] E. Fradkin, S. A. Kivelson, E. Manousakis, and K. Nho, Phys. Rev. Lett. **84**, 1982 (2000).
[19] Quoc M. Doan and Efstratios Manousakis, Phys. Rev. B **75**, 195433 (2007).
[20] K. B. Cooper, M. P. Lilly, J. P. Eisenstein, T. Jungwirth, L. N. Pfeiffer, and K. W. West, Solid State Commun. **119**, 89 (2001).
[21] Shi-Jie Yang and Yue Yu, Phys. Rev. B **68**, 153314 (2003).
[22] K. B. Cooper, J. P. Eisenstein, L. N. Pfeiffer, and K. W. West, Phys. Rev. Lett. **92**, 026806 (2004).
[23] D. V. Fil, Low Temp. Phys. **26**, 581 (2000).
[24] J. S. Langer, Ann. Phys. (N.Y.) **41**, 108 (1967); J. S. Langer, *ibid.* **54**, 258 (1969); J. S. Langer, *ibid.* **65**, 53 (1971); J. S. Langer and L. A. Turski, Phys. Rev. A **8**, 3230 (1973); L. A. Turski and J. S. Langer, *ibid.* **22**, 2189 (1980).
[25] J. M. Kosterlitz and D. J. Thouless, J. Phys. C **6**, 1181 (1973).
[26] For a review of nucleation in soft condensed matter physics see: J. D. Gunton, M. San Miguel, and P. S. Sahni, in *Phase Transitions and Critical Phenomena*, edited by C. Domb and J. L. Lebobowitz (Academic, London, 1983), Vol. 8.
[27] S. M. Alamoudi, Daniel G. Barci, D. Boyanovsky, C. A. A. de Carvalho, E. S. Fraga, S. E. Joras, and F. I. Takakura, Phys. Rev. D **60**, 125003 (1999).
[28] M. B. Voloshin, Yad. Fiz. **42**, 1017 (1985); Sov. J. Nucl. Phys. **42**, 644 (1985).
[29] Yu Lu, *Solitons and Polarons in Conducting Polymers* (World Scientific, Singapore, 1988); A. J. Heeger, S. Kivelson, J. R. Schrieffer, and W. P. Su, Rev. Mod. Phys. **60**, 781 (1988); G. Gruner, *Density Waves in Solids* (Addison-Wesley, Reading, MA, 1994).
[30] D. Boyanovsky and C. Aragao de Carvalho, Phys. Rev. D **48**, 5850 (1993).
[31] D. Boyanovsky, C. A. A. de Carvalho, and E. S. Fraga, Phys. Rev. B **50**, 2889 (1994); C. A. A. de Carvalho, Acta Phys. Pol. B **19**, 875 (1988); C. A. A. de Carvalho, Mod. Phys. Lett. B **3**, 125 (1989); E. S. Fraga and C. A. A. de Carvalho, Phys. Rev. B **52**, 7448 (1995); D. G. Barci, E. S. Fraga, and C. A. A. de Carvalho, Phys. Rev. D **55**, 4947 (1997).
[32] Daniel G. Barci, Marta Trobo, Victoria Fernández, and Luis E. Oxman, Phys. Rev. B **78**, 035114 (2008).